Non-invasive archaeometallurgical approach to the investigations of bronze figurines using neutron, laser and X-ray techniques

Juri Agresti, Iacopo Osticioli, Maria Cristina Guidotti, Nikolay Kardjilov, Salvatore Siano

PII: S0026-265X(15)00260-X
DOI: doi: 10.1016/j.microc.2015.10.030
Reference: MICROC 2289

To appear in: *Microchemical Journal*

Received date: 15 August 2015
Revised date: 22 October 2015
Accepted date: 22 October 2015

Please cite this article as: Juri Agresti, Iacopo Osticioli, Maria Cristina Guidotti, Nikolay Kardjilov, Salvatore Siano, Non-invasive archaeometallurgical approach to the investigations of bronze figurines using neutron, laser and X-ray techniques, *Microchemical Journal* (2015), doi: 10.1016/j.microc.2015.10.030

Non-invasive archaeometallurgical approach to the investigations of bronze figurines using neutron, laser and X-ray techniques

Juri Agresti[(1)*], Iacopo Osticioli[(1)], Maria Cristina Guidotti[(2)], Nikolay Kardjilov[(3)] and Salvatore Siano[(1)]

(1) Istituto di Fisica Applicata "Nello Carrara"-CNR, Sesto Fiorentino, FI, Italy. E-mail: j.agresti@ifac.cnr.it
(2) Soprintendenza per i Beni Archeologici della Toscana, Firenze, Italy.
(3) Helmholtz-Zentrum Berlin für Materialien und Energie GmbH, Berlin, Germany.

Abstract

In the present work, structural imaging and non-invasive compositional analysis have been successfully combined in order to investigate three bronze figurines from the antiquarian collection of the Egyptian Museum of Florence. High resolution neutron tomography was exploited for a thorough reading of the technological features of the mentioned copper alloy statuettes. At the same time portable XRF-XRD, Raman spectroscopy, laser induced plasma spectroscopy, as well as time of flight neutron diffraction, provided a powerful complementary analytical set for achieving reliable surface, depth profile, and bulk analyses. The proposed multi-analytical and non-invasive approach, involving neutron, X-ray and laser techniques, allowed exhaustive identification of the raw materials and interpretation of the crafting processes used by ancient bronze smiths.

Keywords: Multi-analytical, neutron tomography, LIBS, archaeometallurgy, copper alloys

1. Introduction

Ancient Egyptian metallurgy represents a milestone in the development of metal-working and casting practice and its fundamental importance has been recognized since the beginning of the XX century [1, 2]. In the past, bronze figurine production methods and materials have been understood in large degree from extensive studies of ancient samples by means of traditional sampling techniques followed by elemental analysis [3, 4 and references therein] or metallography [5]. Nowadays, a considerable technological advance and the development of best-practices in the preservation of cultural heritages, allow the characterization of object of interest in a non destructive way. Imaging techniques, including standard X-ray or the somehow complementary neutron radiography or tomography (NT) [6], have been applied in the study of metal artifacts of historical interest [7-10]. They can provide information about the material distribution, composition, manufacturing and alteration process. However for a clearer picture about the composition of the materials involved, other analytical techniques are usually needed [11]. Elemental techniques such as X-ray fluorescence (XRF) and ion beam analyses, or molecular techniques such as X-ray diffraction (XRD) have been used in the characterization of Egyptian bronzes surfaces, mostly for the study of corrosion products or surface treatment (patination, gilding, etc..) [12-17]. On the other

side, time of flight neutron diffraction (TOF-ND) can provide compositional and micro structural data averaged over large measurement volumes (in the order of cubic centimeters) [18-21]. Laser induced plasma (or breakdown) spectroscopy (LIPS or LIBS) [22] fills the gap between the above mentioned surface techniques and the TOF-ND bulk analysis, since it provides spatially resolved measurements (in the order of hundred microns) in the form of quantitative elemental depth profiles. Each laser pulse ablates a certain amount of the material, and thus penetrates step by step into the sample. The spectra of the successive laser pulses are processed to obtain the element distribution in depth. LIPS is therefore considered a micro destructive technique (typical ablation diameter of 100-200 microns) but its invasiveness is likely negligible in most applications, even in the cultural heritage domain [23].

Here neutron imaging (NT) and diffraction (TOF-ND) as well as complementary compositional analysis (LIPS, XRF, Raman spectroscopy and XRD) have been successfully combined in order to investigate three bronze figurines from the antiquarian collection of the Egyptian Museum of Florence. This allowed exhaustive identification of the raw materials and interpretation of the crafting processes used by ancient bronze-smiths. The selected artifacts presented some peculiarities which made them representative of a broad class of archaeometric investigations. Preliminary X-radiographic analysis allowed arguing that one of them, representing the goddess Neith, contained intact casting cores, while another one, representing a nursing Isis, was emptied of the casting cores from visible openings, and the third, representing the Horus Falcon, contained some residual materials. However X-radiography did not allow a sufficient image contrast needed in order to decipher the manufacturing procedures and state of conservation. Casting cores in Egyptian bronzes typically were left intact (see for example [24]), unless the pieces were intended to function as sarcophagi, which is the case for many of the hollow-cast animal figures. As an example, which is of interest for in the present investigation, several falcon bronze sculptures in the Walters Art Gallery collection in Baltimore, Maryland, were analyzed using thermal neutron radiography and most of them seemed to contain bird remnants or mummy bundles [25]. This organic material showed up in the neutron radiograph because some of the light chemical elements present in them, particularly calcium, nitrogen and hydrogen, posses a high neutron attenuation coefficient. However, it must be stressed that a clear identification of bird bones was only possible in one sample thanks to a direct visual inspection via an endoscope inserted into a small hole in the head of the falcon. Our falcon sample does not present any aperture and we exploited for the first time high-resolution neutron tomography and TOF-ND in order to visualize such remnants deposited in an inaccessible bronze cavity, and give some insights on their composition.

2. Materials and methods

The samples used in this work to demonstrate the potentialities of the integration of the above mentioned techniques in archaeometallurgical studies are three bronze figurines from the Egyptian collection of the Archaeological Museum of Florence (Fig. 1). The largest one (inv. N.8401) was a bronze falcon (15 x 6.5 x 15 cm) on a wooden base (7.5 x 10 x 24 cm), which was a standard representation of the god Horus in ancient Egypt. It has unknown origin and was inherited by the museum from Bartolucci legacy in 1892. The surface appeared of dark brown/ reddish tone with evident signs of corrosion especially on the left side where earthy material and green corrosion

compounds are mixed. Nevertheless fine details of the crafting process such as the engraved feathers were still visible and overall it was in reasonably good state of conservation. The second figurine represented a seated nursing Isis (*Isis Lactans*) (13.5 x 4.7 x 6.5) cm). Also this sample has unknown origin and was inherited by the museum from Bartolucci legacy in 1892. It is in the position of breastfeeding the baby god Horus, which is now missing. Other parts are probably missing, such as the protruding *Uraeus* over her forehead, where a square hole is visible, and two cow horns enclosing a sun-disk surmounting the present *modius* adorned with *Uraei*. A tang underneath the legs would have been used to secure the statuette to a base. The surface of the bronze figurine appeared completely covered by a dark almost black patina with large area of reddish corrosion products. Moreover some traces of gilding were visible on the face and in the two parts of the finely engraved wig falling onto the chest. Ancient Egyptian black-patinated copper alloys has attracted much attention in the last century and the debate on their production process is still open [13, 15, 16, 26]. We will address this issue later. The last figurine represents a seated Neith (13.5 x 3 x 5 cm), warrior goddess, wearing the red crown of the Lower Egypt. Two tenons, one under the legs and one under the feet, were probably inserted into a missing throne. Its provenance was not known and was acquired by the museum in 1824 from the private Nizzoli collection. The left arm was broken but the surface of the figurine appeared well preserved, with limited corrosion phenomena. The three bronze figurines were stylistically dated to the Late Period (664-332 B.C.).

Neutron tomography was performer at the imaging facility CONRAD II at the Hahn-Meitner research reactor at Helmholtz-Zentrum Berlin (HZB) [28, 29]. The cold neutron beam (wavelength range 1.5 Å -10 Å with peak at 2.5 Å) is directed to the tomography set-up via a curved neutron guide which provides a flux density of about $2 \cdot 10^9$ n/(cm^2 s). Beam collimation was performed by means of pinhole geometry with a 3cm diameter circular pinhole resulting in a beam collimation ratio (L/D) of 333. A conventional 100 μm thick 6LiF:ZnS scintillation screen has been used along with a CCD camera with 2048×2048 square pixels (size of 13.5 μm). The imaging set-up allowed achieving a spatial resolution of about 200 μm with a field of view (FOV) of 20x20 cm and an effective pixel size of 107 μm. The sample was rotated stepwise around a fixed vertical axis (500 steps for 360° rotation), whereby for each rotation angle a projection image was recorded with exposure time of 50s. The set of projections have been processed by commercial reconstruction software in order to obtain the 3D distribution of the attenuation coefficients in the investigated sample volume.

The time of flight neutron diffraction experiments have been performed on the Italian Neutron Experimental Station (INES) [30], situated at the ISIS spallation neutron source of the Rutherford Appleton Laboratory, UK. INES diffractometer is equipped with nine detector banks covering 2θ angles from 20° to 163° in the horizontal scattering plane. Neutrons scattered by the sample produce nine separate diffraction patterns (partially overlapping) each of them covering a different d-spacing range with different resolution. The incoming neutron beam of 34x34 mm^2 was shaped as shown in Fig. 1 using adjustable jaws and beam monitoring device in order to select specific region of interest for the analysis and the acquisition time was in the range 1-3 hours for each measurement. Let us point the attention to the fact that TOF-ND measurements on extended object like these hollow bronze figurines are subjected to some systematic effects which could make the quantitative phase analysis quite problematic. For an extended object, the incident beam will

diffract from different materials that may be located at different positions along the incident beam path. The diffraction data obtained from hollow closed sample are effectively being produced from the interaction of the neutron beam with the walls of the sample, displaced with respect to the centre of the diffractometer in the direction of the beam, resulting in two diffracted peaks, one from each side of the sample. The resolution of the instrument is sufficient to reveal this effect as peak broadening or splitting according to the following equation [31]

$$\frac{\Delta d}{d} = \frac{\Delta t}{t} = x\left(\frac{1-\cos 2\theta}{L_1 + L_2} + \frac{\cos^2\theta}{L_2}\right) \cong x\frac{\cos^2\theta}{L_2}$$

Where x is the sample displacement away from the ideal sample position in the direction parallel to the beam, Δt is the TOF difference with respect to the TOF t of the centered sample,2θ is the scattering angle, and L_1 e L_2 are the primary and secondary flight paths of the diffractometer, respectively. The approximated expression on the right is justified if the primary flight path of the diffractometer is much longer than the secondary one, which is the case of the INES instrument ($L_1 = 22.8\,m, L_2 = 1\,m$). The dependence on the scattering angle makes this effect more pronounced for the forward scattering banks, leading to a relative d-spacing shift of about 6% for the detector at 20° and target's sides separation of 6 cm. The same double walls interaction produces a relative d-spacing shift of 1.2 10^{-3} in the backscattering bank at 163°, which is the same order of magnitude as the instrumental resolution. Therefore in the analysis of the diffraction patterns from the Egyptian statuettes, the lattice parameter of the bronze α-phase was extracted from the data of the backscattering bank and the quantitative multi-phase analysis using the Rietveld refinement method has been limited to the first three banks in the case of the bronze falcon. Conversely, the small transverse dimensions of the Neith sample, allowed the use of eight banks for quantifying the typical metal and alteration phases of the present copper alloy artefact as well as the mineral phases constituting its core materials. The observed patterns were analyzed according to the established procedures of the Rietveld method using the software GSAS [32] with the EXPGUI interface [33].

The INES beamline also provides neutron resonance capture analysis (NRCA) [34] by using an Yttrium-Aluminum-Perovskite (YAP) crystal coupled to a photomultiplier tube and placed on top of the same sample tank of the diffractometer [35]. The neutron resonances are determined with the time of flight (TOF) technique by detection of the prompt γ-radiation emitted immediately after capture. The time-of-flight spectra (see Fig. 6) can be converted in standard intensity-energy form by using the expression $E = \frac{1}{2}m_n\left(\frac{L}{t}\right)^2$, where m_n is the neutron mass, L is the path length and t is the measure time of flight. Here NRCA measurements have been used for semi-quantitative estimation of elements with neutron absorption resonances in the epithermal energy region (3-4000 eV with limited sensitivity in the keV range due to the high background and low neutron flux at this energy). In order to perform a semi-quantitative analysis, we estimated the relative isotopic concentration by weight for a few of the isotopes recognized in the sample, from the relative intensities of the peak maxima, I_p. For weak resonances and in the thin sample approximation, the intensity ratio of two resonances in the flux-normalized resonance spectrum is related to the elements weight fraction by a simple equation

$$\frac{W_i}{W_k} = \frac{I_{pi} W_{Mi} a_k \sigma_{rk}}{I_{pk} W_{Mk} a_i \sigma_{ri}}$$

where W_M is the element molar mass, a is the isotopic abundance and σ_r is the capture resonance cross section. The selected resonances were 994 eV for ^{63}Cu, 38.8 eV for ^{117}Sn, 5.19 eV for ^{109}Ag, 21.38 eV for ^{123}Sb, 318.6 eV for ^{75}As, and 3063 eV for ^{207}Pb. Resonances cross sections were taken from public databases [36].

LIPS measurements were performed using the homemade portable device described in details in [37]. It is equipped with a Q-Switched Nd:YAG (1064 nm) laser, emitting pulses of about 8 ns at maximum energy of 50 mJ/pulse. It is focalized to the target via a 60 mm focal length lens producing a spot diameter at its surface of about 110μm (peak intensity of about 70 GW/cm^2). The plasma emission is collected through off-axis parabolic mirrors and coupled via optical fibers to the entrance slits of a set of four high resolution compact Czerny-Turner spectrometers (2,400 grooves/mm) equipped with CCD linear array detectors, which covered the spectral range between 200-630 nm with resolution of about 0.1 nm. A dedicated software code controls the timing sequence of the trigger signals to the laser and to the spectrometer-detector (acquisition delayed of 500 ns and effective integration time of ca. 3 μs, as determined by the plasma lifetime [37]) and processes the spectra for the qualitative and quantitative LIPS analysis. The device is calibrated for quantitative analysis of copper alloys containing Sn, Pb, Zn, Fe, Ni and As, also taking into account the dependence of calibration curve on the depth of the microcrater excavated by laser ablation [38]. The estimated detection limits were about 0.5 wt% for As, and about 0.1 wt% for the other elements (weight percentages relative to copper). Several quantitative elemental depth profiles were collected for each figurine, using at least 2000 laser pulses in each measurement site. This corresponds to a depth of the microcrater in the range of 700-1500 μm, according to the samples composition and mineralization of the surface. The typical behavior of the depth profile of archaeological artifacts presents an initial modulation zone which is due to surface alteration effects produced mainly by corrosion phenomena [39], and an innermost part where the depth profile plots gradually approach to a relatively stable value, which represent the bulk composition. The measurement of exogenous elements (Ca and Si), which likely come from the burial environment and weathering conditions, also help to discriminate the corrosion layer from the bulk material. Thus, the composition of the latter is calculated by averaging about 500 measurements along the inner most part of the depth profiles where the signals stabilize and the contribution from exogenous material has disappeared.

The complementary surface analysis, Raman spectroscopy and XRF-XRD, where performed with commercial portable instruments. The Raman spectrometer (model I-Raman, B&W Tek, DE, USA) is a compact device using an excitation wavelength of 785 nm and a TE cooled detector (2048 pixels), which covers the spectral range of 260–3200 cm^{-1} with a resolution of 6 cm^{-1}.

The XRF-XRD instrument, produced by Assing s.p.a., consists of an X-ray tube and a X-ray detector moving on θ-θ goniometer. The X-ray tube features a gold (Au) transmission target, a maximum input voltage of 50 kV and a maximum current of 200 μA. The Si-drift detector (SDD) has a resolution of 165 eV (FWHM @ 5.9 keV). X-ray tube and detector were equipped with a cylindrical collimator the former and a pair of vertical slits the latter, of 1mm internal diameter and 1mm width respectively. With these parameters and a step of 0.1° in 2θ-scan (3 seconds acquisition

per step), we achieved a resolution for XRD measurements of about 1% (Δd/d @ d[100Si] of a silicon wafer).

3. Results and discussion

3.1 Falcon 8401

High resolution neutron tomography allowed identifying several features characteristic of the production process such as the numerous core pins traversing the bronze walls, which were used for preventing any movement of the core with respect to the external mould while pouring the molten metal, after the wax was run off. Fig. 2 shows the tomographic sections where the core pins have been identified. Most of the core pins appear also on the outer surface, allowing taking measurements to identify the composition of them. XRF and LIPS (8401_1) measurements on the two pins on the back of the falcon identified iron as the major component and Raman measurements identified hematite and goethite as the actual mineral phases. Therefore the core pins appeared to be made of iron almost completely transformed into rust, as the relatively high neutron attenuation in the tomography suggested (see Fig. 2 and Fig. 3). The outer surface of the bronze falcon appears highly corroded and the tomographic sections point out a thick layer (around 1 mm) of highly absorbing compounds, probably rich in hydrated oxides, copper chlorides and other copper corrosion product rich in hydrogen and carbon. XRF-XRD analysis on the greenish area on the left side, which appeared to be highly attenuating for neutrons, identified paratacamite ($Cu_2Cl(OH)_3$) and nantokite (CuCl) as the major corrosion compounds. The casting core appeared to be almost completely removed from the small almost square aperture (2.5x2.5 cm) in the underside of the Horus, behind the legs, now sealed with a bronze plate. This was a common practice in ancient Egypt because very often these hollow bronze figurines were filled with animal remnants or small mummies for religious purpose. We will address this issue in the following. Some remnants of the original casting core are still present inside the falcon legs, where the tools used to remove the earthy material could not access. Top right of Fig. 3 shows a section of the NT where the compact and rather homogeneous casting core remnants in the lower part of the left leg are well distinguished from the incoherent and inhomogeneous material distributed inside the falcon. The appearance of this material is very different from an earthy one, resembling more a mixture of fibrous, laminar, and elongated fragments, which may suggest the possibility of being the remnants of small bones, fragments of textile and other organic residues. A precise identification using tomographic reconstruction was not possible because the material appears mostly fragmented and the resolution of the measurements did not allow a satisfactory segmentation of the different components. In absence of a direct access to the material we could only exploit neutron diffraction analysis to gain some insights on the composition of it. In particular we used two TOF-ND measurements performed on the body of the falcon where e high concentration of this material was observed. Fig. 4b shows the comparison of the diffraction spectra acquired on the central part of the

body (Body_2), the middle part of the tail (Body_1) in correspondence of the sealed aperture, and a reference measurement on the head of the falcon which is empty from any unidentified material. In the spectrum Body_1 some peaks (marked by arrows) could be related with the most intense peaks of hydroxyapatite ($Ca_5(PO_4)_3(OH)$), a calcium phosphate salt which could refer to the inorganic component in calcified hard tissues (e.g., boneand teeth) of vertebrates. In fact the major constituent of bones is a calcium phosphate mineral that is similar in composition and structure to minerals within the apatite group, and hydroxyapatite has been identified as the best approximation of it, although with a highly defective/poorly crystallized structure. Furthermore three peaks on the diffraction pattern of Body_2, which are not present in the reference spectrum, could pertains to the most intense peaks of sodium carbonate ($Na_2(CO_3)$) which could be related to the natron use in Egyptian practice of mummification. Moreover a small broad peak at about 3.9 Å could be observed in the diffractograms of the body, which could be compatible with the 002 reflection of cellulose. All these data could support the hypothesis that the falcon was filled with a mixture of bones fragments, textile fibers, possible natron material and perhaps small pieces of other organic and inorganic material. However considering the large number of mineral phases possibly present on such complex artifact, which could produce the observed peaks, and a possible peak shift due to the mentioned off-center effect ($\Delta d/d \cong 0.009\ x(cm)$ for $2\theta=37°$, where x is the off-center displacement), a univocal identification was not possible. For example the peaks attributed above could actually be assigned to bronze corrosion compounds such as covellite (CuS), cassiterite (SnO_2), brochantite ($Cu_4SO_4(OH)_6$) and to lead degradation products (PbO, $PbCO_3$ and $Pb(CO_3)_2(OH)_2$) which could be associated with the soldering material of the bronze plate in the aperture. Let us remark that the analysis did not allow a clear identification of the inner materials but gave some hints for future more detailed investigation focused on their identification.

The average alloy composition measured with LIPS (Table 1) in the innermost part of the depth profiles is in good agreement with the results of TOF-ND (Fig. 4a1 and Table 2), taking into account that the mentioned effect related to the target size limits the potentialities of the multibank Rietveld refinement. The bulk composition was reached by laser sampling after several thousand pulses because of the mentioned corrosion effects which alter the composition of the outer bronze layer. One of the measured profiles is shown in Fig. 5 on top. It presents the typical behavior of the elemental profiles of a layered structure formed by copper compounds and cuprous oxides on surface, followed by an altered layer characterized by selective copper dissolution and leaching phenomena, and finally the bulk material [39]. As a confirmation of the relatively high degree of mineralization of the falcon surface, TOF-ND measured a consistent weight fraction of cuprite all over the falcon body. One example of the measured NRCA spectra is displayed in Fig. 6. The semi-quantitative NRCA measurements (Table 3) detected small abundance of elements such as silver (Ag) and antimony (Sb), which were not quantified with the other techniques. Moreover, the high amount of lead detected in correspondence of the sealed aperture, supports the hypothesis that the bronze plate was attached to the aperture with lead filler, which is now almost completely corroded. In fact, the light gray level of the filler in Fig. 3 bottom-left, could corresponds to high attenuating compounds like hydrocerussite ($Pb(CO_3)_2(OH)_2$) whose diffraction peaks could be identified also in the diffractogram Body_1 of Fig. 4b.

3.2 Neith

Neutron tomography of Neith confirmed that the bronze figurine contained the original casting core that remained sealed inside the metal body (Fig. 7). The casting core appeared of a very rough shape, with all the protruding parts like head and arms, actually modeled directly on wax. The main components of the mineral phases of the casting cores measured by TOF-ND correspond to quartz (SiO_2), the calcium feldspar anorthite ($CaAl_2Si_2O_8$), and the alumino-silicate mullite ($Al_6Si_2O_{13}$) (see Table 2). The presence of high temperature phases like mullite and the absence of diffraction signals from clay mineral compounds (i.e. kaolinite and montmorillonite), suggests that the casting cores were fired at high temperature, probably above 1000°C. Although the presence or absence of specific mineral phases in the casting core material can provide some information on the production technology, it must be recalled that for an initial clay-sand-pebble mixture of given chemical and mineralogical composition, the final mineral assemblage of the fired mould is strongly influenced by firing temperature and atmosphere [40] (which are not known) and is not possible in general to univocally deduce the original materials from that. Several core pins were identified through the tomographic slices, as reported in Fig. 7, and the combined analysis XRF and Raman on some of them appearing on the surface of the statuette confirmed the composition as rusted iron, with strong preponderance of iron oxide/hydroxides. The central part of the body (chest) presented highly mineralized area, which are evident by visual inspection (reddish area), tomographic sections and neutron diffraction data (high amount of cuprite), while the head appeared well preserved and homogeneous in composition. The alloy composition measured by LIPS (Table 1) and TOF-ND (Table 2) corresponds to a high leaded bronze, with lead content of about 14 wt%. LIPS quantitative analysis also measured about 2.1% of tin and 1.1% of arsenic. On the other side, neutron diffraction (see Fig. 4a2) measured a little amount of the copper-arsenide compound identified as algodonite (Cu_6As), which is one of the possible Cu-rich eutectic phases of the Cu-As system [41]. The rapid and inhomogeneous cooling of the alloy during the casting process could have originated this phase. This is supported also by the evidence of a larger presence of this phase in the thin walls of the body, with respect to the amount measured in the solid head. However the amount of arsenic contained in algodonite alone does not explain the value measured by LIPS, in fact corresponds to less than 0.2% of the total copper content. It was reasonable to expect that the Cu-like (Fm3m) phase measured by TOF-ND was actually a ternary α-(Cu-Sn-As) phase, meaning a substitutional solid solution of Sn and As in the α-(Cu) phase. Following the procedure adopted previously [24], we assumed that the lattice parameter of the α-(Cu-Sn-As) phase can be expressed as a linear combination of the individual Sn and As contribution

$$a_{meas} = a_0 + k_{Sn}x_{Sn} + k_{As}x_{As}$$

where a_{meas} and a_0 are the measured and pure copper lattice constants respectively, x are the weight concentration in the alloy, and $k_{Sn} = 0.00584$ Å and $k_{As} = 0.00513$ Å are the phenomenological coefficient calculated in [42]. In this equation the concentrations of Sn and As are in principle unknown and therefore we used the LIPS measured value of x_{Sn} in order to calculate the expected contribution of As to the lattice parameter. The result of the calculations, including the contribution from algodonite, reproduced exactly the 1.1% of As in the total alloy composition measured with LIPS. NRCA analysis (Table 3) provided congruent data on the concentration of the major (Cu, Pb) and minor (Sn, As) elements and detected trace amounts of Sb and Ag.

3.3 Isis Lactans

Fig. 8 shows some representative vertical/horizontal slices of the tomographic analysis of the Isis figurine, together with a section of the 3D reconstructed rendered volume. From these we could extract several information related to the manufacturing process: the figurine was a single hollow cast piece with solid arms and feet; three core pins were identified, one in the chest, one in the legs and one on the lower back area (not shown); one small (about 9x3 mm) repair patch, probably due to a casting defect, was identified on the right leg. Also in this case the core pins composition was identified by combining the elemental information of XRF/LIPS, which detected large amount of iron, with the molecular information of Raman spectroscopy, which clearly identified goethite as the principal mineral phase of the rusted pins (Fig. 9 b)). The original casting core was almost completely removed from inside the figurine, except that for few remnants inside the thigh (visible in the 3D model of Fig. 8) and in the lower part of legs. This sample was not analyzed at the INES beamline and therefore no TOF-ND and NRCA data are available. The alloy compositions measured with LIPS were, Sn 2.2 wt%, Pb 15 wt% and As 2.3 wt% for the body and Sn 0.7wt%, Pb 14.8 wt%, As 2.2wt% and Ni 0.4 wt% for the repair patch. Some of the peculiarities of this bronze figurine are related to its surface. In fact it appeared completely covered by a relatively uniform and compact black patina, alternated to reddish areas. Moreover the face and hairs presented visible traces of gilding (see Fig. 10). Numerous XRD (one of them is shown in Fig. 9 a)) and Raman spectroscopy univocally identified the black compound as tenorite (CuO) and the reddish one as the more common cuprite (Cu_2O). In general, tenorite formation in corrosion layers of archaeological bronze is disfavored with respect to cuprite, but is likely produced on heating [43]. The present uniform distribution on the entire surface and the preservation of fine details such as the regular pattern of thin lines representing hairs, support the hypothesis that the statuette has been subjected to intentional black patination by heating it in order to form a homogeneous layer of tenorite. Some parts of the figurine were then gilded by using thin gold leaves attached with adhesives like animal glue. The hypothesis of fire-gilding (Hg-based amalgam) was disproved by the fact that neither LIPS nor XRF detected any signal of mercury in correspondence of the gilding remnants. The reduced dimensions of the bronze figurine allowed performing also some analysis using the scanning electron microscope with microanalysis (ESEM-EDX), which confirmed the results mentioned above obtained by visual inspection through the optical microscope and the elemental analysis of portable instruments.

3.4 Casting technique

The tomographic data, combined with the compositional analysis, allowed drawing some general conclusions regarding the casting technique and the used material. The three figurines were cast through the well-known lost wax technique. This is supported by the very thin walls and by the evidence of several core pins. A direct casting procedure was used, which started with the production of the inner casting molds with clay-sand mixture, presenting a rough shape of the final object. The inner core could also have resulted by some sort of copy process from models. Afterwards iron pins were inserted into the core in order to hold it in position inside the mold after

the wax has been melted out and while the molten bronze was being poured in. Wax was applied around the core structure and sculpted into the finished design. Channels and vents were probably added to facilitate the flow of molten metal and allow gases to escape. The model was then invested in clay and earthy materials to form the outer mold and all the assemblage was finally fired in order to harder the clays and melt/burn the wax. The molten metal was then poured into the mold to replace the wax model and after a cooling time the mold was opened and the bronze figurine underwent the finishing and eventually the removal of the casting cores. The high lead content measured in the alloy of the three bronze figurines suggested this element was intentionally added in order to improve the fluidity of the melted metal during the casting process.

5. Conclusions

In this work high resolution neutron tomography was combined with neutron, laser and X-ray non-invasive compositional analysis for thoroughly investigating three hollow-cast bronze figurines. The data obtained with each technique complemented each other and enabled a meaningful interpretation of the findings. In particular, neutron tomography evidenced a set of characteristic technological features, enabling the interpretation the casting procedure, which was similar for the three Egyptian bronzes. On the other side, the combination of elemental (LIPS, XRF) and crystal analysis (TOF-ND, Raman, XRD) allowed the identification of the raw materials used in casting (alloy compositions, core pins), of the main corrosion product and eventually of surface treatment like patination and gilding. Furthermore, in the interior of the hollow bronze falcon, in addition to the remains of the original casting cores, neutron tomography revealed the presence of some incoherent and mostly fragmented material, resembling small bones, fragments of textile and other organic residues. TOF-ND measurements gave some support to this hypothesis, but further investigations are needed to settle the issue. Moreover the integration of neutron and LIPS (depth profile) analysis was crucial for a reliable quantification of the complex alloy composition of these archaeological bronzes, where, mineralization and corrosion phenomena limit other non-destructive techniques.

The proposed multi-analytical approach represents a methodology of general valence that can be applied to other archaeometallurgical studies involving hollow-cast archaeological bronzes.

Acknowledgements

This work has been supported by the European Commission under the 7th Framework Programme through the “Research Infrastructures” action of the “Capacities” Programme, CP-CSA_INFRA-2011-1.1.17 Number 233883 NMI3 II and by the CNR Project SM@RTINFRA-SSHCH, (Art. 5 DM n. 949/Ric 19/12/2012). The authors would like to thank Marcello Miccio (IFAC-CNR and Soprintendenza per i Beni Archeologici della Toscana-MiBAC) for having provided the X-radiographies.

References

[1] W.M.F. Petrie, The Arts and Crafts of Egypt, Foulis, Edinburgh, 1910.

[2] H. Garland and C.O. Bannister, Ancient Egyptian Metallurgy, Griffin, London, 1927.

[3] J. Riederer, Metal analysis of Egyptian bronzes, Revue d'Archeometrie, 3 (1981) 239-245.

[4] J. Ogden, Metals, in: P.T. Nicholson, I. Shaw (Eds.), Ancient Egyptian Materials and Technology, Cambridge University Press, Cambridge, 2000, pp. 148-176.

[5] D.A. Scott, Metallography and microstructure of ancient and historic metals, Getty Conservation Institute, Singapore, 1991.

[6] F. Casali, X-ray and Neutron Digital Radiography and Computed Tomography for Cultural Heritage, in Physical Techniques in the Study of Art, Archaeology and Cultural Heritage, v. 1, ed. by D. Bradley and D. Creagh, Elsevier, Amsterdam, 2006, pp. 41–123.

[7] E. Deschler-Erb, E. H. Lehmann, L. Pernet, P. Vontobel and S. Hartmann,The complementary use of neutrons and X-rays for the non-destructive investigation of archaeological objects from Swiss collections. Archaeometry, 46 (4) (2004) 647-661.

[8] J. Rant, Z. Milič, J. Istenič, T. Knific, I. Lengar and A. Rant, Neutron radiography examination of objects belonging to the cultural heritage, Appl. Radiat. Isotopes, 64 (2006) pp. 7-12.

[9] R. Van Langh, E. Lehmann, S. Hartmann, A. Kaestner and F. Scholten, The study of bronze statuettes with the help of neutron-imaging techniques, Anal. Bioanal. Chem., 395 (2009) pp. 1949–1959.

[10] E. H. Lehmann, E. Deschler-Erb and A. Ford, Neutron tomography as a valuable tool for the non-destructive analysis of historical bronze sculptures, Archaeometry, 52 (2010) pp. 272-285.

[11] R. Van Langh, J. Jones, G. Burca, W. Kockelmann, S.Y. Zhang, E. Lehmann, M. Estermann and A. Pappot, New insights into alloy compositions: Renaissance bronze statuettes by combined neutron imaging and neutron diffraction techniques, J. Anal. At. Spectrom., 26 (2011) 949.

[12] A. Smith, H. Botha , F.C. de Beer, E. Ferg, The examination, analysis and conservation of a bronze Egyptian Horus statuette, , Nuc. Inst. Met. Phys. Research A 651 (2011) 221–228.

[13] E. Delange, M. Aucouturier,, M.-E. Meyohas, The statue of Karomama, a testimony of the skill of Egyptian metallurgists in polychrome bronze statuary, J. Cult. Herit., 6 (2005) 99–113.

[14] V. K. Gouda, G. I. Youssef and N. A. Abdel Ghany, Characterization of Egyptian bronze archaeological artifacts, Surf. Interface Anal., 44, (2012) 1338–1345.

[15] F. Mathis, E. Delange, D. Robcis, and M. Aucouturier, HMTY-KM (black copper) and the Egyptian bronzes collection of the Musée du Louvre, Journal of Cultural Heritage, 10, (2009) 63–72.

[16] W. Mohamed and S. Darveesh, Ancient Egyptian black-patinated copper alloys, Archaeometry 54, 1 (2012) 175–192.

[17] M. Ghoneim, An egyptian partially gilded bronze group statue: examination and analysis, Archaeometry 57, Suppl. 1 (2015) 130–146.

[18] W. Kockelmann, A. Kirfel and E. Hähnel, Non-destructive Phase Analysis of Archaeological Ceramics using TOF Neutron Diffraction, J. Archaeol. Sci., 2001, 28, 213-222.

[19] S. Siano, W. Kockelmann, U. Bafile, M. Celli, M. Iozzo, M. Miccio, O. Moze, R. Pini, R. Salimbeni, M. Zoppi, Quantitative multiphase analysis of archaeological bronzes by neutron diffraction, Appl.Phys. A, 2002, 74, S1139.

[20] S. Siano, L. Bartoli, W. Kockelmann, M. Zoppi, and M. Miccio,"Neutron metallography" of archaeological bronzes, Physica B: Cond. Matt. , 2004, 350, 123-126.

[21] F. Grazzi, F. Civita, A. Williams, A. Scherillo, E. Barzagli, L. Bartoli, D. Edge, M. Zoppi, Ancient and historic steel in Japan, India and Europe, a non-invasive comparative study using thermal neutron diffraction. Anal. Bioanal. Chem. 400 (2011) 1493–1500.

[22] R. Noll, Laser-Induced Breakdown Spectroscopy : fundamentals and applications, Springer-Verlag, Berlin- Heidelberg, 2012.

[23] D. Anglos and V. Detalle, Cultural Heritage Applications of LIBS, in S. Musazzi and U. Perini (Eds.), Laser-Induced Breakdown Spectroscopy. Springer Series in Optical Sciences 182, Springer-Verlag, Berlin Heidelberg, 2014, 531-554.

[24] J. Agresti, I. Osticioli, M. C. Guidotti, G. Capriotti, N. Kardjilov, A. Scherillo, S. Siano, Combined neutron and laser techniques for technological and compositional investigations of hollow bronze figurines, J. Anal. Atom. Spectrom., 30 (2015) 713-720.

[25] P. Jett, S. Sturman, and T.D. Weisser, A study of the egyptian bronze falcon figures in the Walters Art Gallery, Studies in Conservation, 30, (1985) 112-118.

[26] P. T. Craddock, and A. Giumlia-Mair, Hsmn-Km, Corinthian bronze, Shakudo: black patinated bronze in the ancient world, in Metal plating and patination (eds. S. La Niece and P. T. Craddock), (1993) 101–27, Butterworth-Heinemann, London.

[28] N. Kardjilov, A. Hilger, I. Manke, M. Strobl, M. Dawson, S. Williams and J. Banhart, Neutron tomography instrument CONRAD at HZB, Nuc. Inst. Met. Phys. Research A, 651 (2011) pp.47-52.

[29] N. Kardjilov, A. Hilger, I. Manke, J. Banhart, CONRAD-2: The neutron imaging instrument at HZB, Neutron News, 25 (2) (2014) pp. 23-26.

[30] S. Imberti, W. Kockelmann, M. Celli, F. Grazzi, M. Zoppi, A. Botti, A. Sodo, M. Leo Imperiale, M. de Vries-Melein, D. Visser and H. Postma, Neutron diffractometer INES for

quantitative phase analysis of archaeological objects , Meas. Sci. Technol., 19 (2008) 034003.

[31] X.-L. Wang, Y. D. Wang, and J. W. Richardson, Experimental error caused by sample displacement in time-of-flight neutron diffractometry, J. Appl. Cryst., 35, (2002) pp. 533-537.

[32] A. C. Larson and R. B. Von Dreele, General Structure Analysis System (GSAS), Los Alamos National Laboratory, Report LAUR86-748, 2004.

[33] B. H. Tobyy, EXPGUI, a graphical user interface for GSAS, J. Appl. Crystallogr., 2001, 34, 210–213.

[34] H. Postma, P. Schillebeeckx, and R. B. Halbertsma, Neutron resonance capture analysis of some genuine and fake etruscan copper alloy statuettes, Archaeometry 46, 635 (2004).

[35] A. Pietropaolo, G. Gorini, G. Festa, E. Reali, F. Grazzi, and E.M. Schooneveld, A Neutron Resonance Capture Analysis Experimental Station at the ISIS Spallation Source, Appl Spectrosc., 64 (9), (2010) pp. 1068-1071.

[36] Nuclear Data Services, International Atomic Energy Agency, https://www-nds.iaea.org/

[37] J. Agresti, A. A. Mencaglia and S. Siano, Development and application of a portable LIPS system for characterising copper alloy artefacts, Anal. Bioanal. Chem, 395 (2009) pp. 2255-2262.

[38] J. Agresti and S. Siano, Depth-dependent calibration for quantitative elemental depth profiling of copper alloys using laser-induced plasma spectroscopy, Appl. Phys. A, 117 (2014) pp. 217-221.

[39] L. Robbiola, J.M. Blengino, and C. Fiaud, Morphology and mechanisms of formation of natural patinas on archaeological Cu–Sn alloys, Corros. Sci., 40 (12) (1998) pp. 2083–2111.

[40] T. Tarvornpanich, G. P. Souza, and W. E. Lee, Microstructural Evolution in Clay-Based Ceramics II: Ternary and Quaternary Mixtures of Clay, Flux, and Quartz Filler, J. Am. Ceram. Soc., 91 (2008) pp. 2272-2280.

[41] P.R. Subramanian and D.E. Laughlin, The As-Cu (arsenic-copper) system, Bulletin of Alloy Phase Diagrams, 9 (1988) pp. 605-617.

[42] F. Grazzi, L. Bartoli, S. Siano and M. Zoppi, Characterization of copper alloys of archaeometallurgical interest using neutron diffraction: a systematic calibration study, Anal. Bioanal. Chem, 397 (2010) pp. 2501-2511.

[43] D. A. Scott, Copper and bronze in art: corrosion, colorants, conservation, Getty Publications, Los Angeles CA, 2002.

Table 1: Average alloys compositions measured with LIPS

Site	Sn (wt%)	Pb (wt%)	Fe (wt %)	Ni (wt%)	As (wt%)
8401_2	7.0 ± 0.8	8.3 ± 1	0.16 ±0.05	0.3 ± 0.1	
8401_3	5.9 ± 0.6	7.1 ± 0.7	0.12 ± 0.04	0.3 ± 0.2	
8401_4	7.6 ± 1	7.9 ±0.7	0.28 ±0.09	0.3 ±0.1	
8401_5	6.7 ±0.8	8.7 ±0.7	0.3 ±0.1	0.3 ±0.1	
8401_6	5.4 ± 0.6	7.2 ±0.6	0.22 ±0.06	0.4 ±0.1	
8401_7	7.1 ±0.8	7.5 ±0.7	0.16 ±0.04	0.4 ±0.1	
IL_1	2.0 ± 0.2	16.1 ± 1.3			2.4 ± 0.5
IL_2	2.3 ± 0.3	15.6 ± 1			2.3 ±0.6
IL_3	2.5 ± 0.2	15.0 ± 0.6			2.3 ±0.4
IL_4	2.1 ± 0.2	13.0± 0.6			2.2 ± 0.4
IL_5	0.8 ± 0.3	14.8 ± 1.6		0.4 ± 0.2	2.2 ± 0.8
N_1	2.1 ± 0.2	13.3 ± 2.4			0.7 ± 0.4
N_2	2.2 ± 0.2	8.6 ± 1.6			1.3 ± 0.7
N_3	2.1 ± 0.2	14.4 ± 1.1			1.2 ± 0.6
N_4	2.1 ± 0.5	14.3 ± 1.9			1.4 ± 0.6

Table 2: Quantitative multiphase analysis from TOF-ND data.

site	α-bronze	a (Å)	Sn_{eq}% in bronze	Pb	Cu_2O	Quartz	Anhortite	Mullite	Cu_6As
8401 head	90	3.646	5.4	7	3				
8401 body_3	88	3.652	6.4	8	4				
Neith head	85	3.635	3.5	14					1
Neith body	66	3.635	3.5	10	7	9	3	3	2

Table 3: Weight ratios (semi-quantitative) of minor elements with respect to Cu, obtained by NRCA analysis

Site	Sn/Cu	Ag/Cu	Sb/Cu	As/Cu	Pb/Cu
8401 head	0.07	$3.5\ 10^{-4}$	$4.3\ 10^{-4}$	0.003	0.06
8401 body_1	0.06	$3.8\ 10^{-4}$	$2.6\ 10^{-4}$	0.004	0.12
8401 body_2	0.08	$5.8\ 10^{-4}$	$2.3\ 10^{-4}$	0.005	0.09
8401 body_3	0.06	$3.2\ 10^{-4}$	$2.1\ 10^{-4}$	0.004	0.06
Neith head	0.03	$2\ 10^{-4}$	$1.6\ 10^{-3}$	0.013	0.19
Neith body	0.03	$2\ 10^{-4}$	$1.5\ 10^{-3}$	0.014	0.15

Fig. 1: Bronze figurines analyzed in this work. Left: Horus falcon (inv. 8401). Middle: Isis Lactans, Right: Neith. Dashed squares mark the TOF-ND analysis. LIPS measurements are numbered for each sample and underlined numbers indicate measurements done on the backside. The shown X-radiographies have been performed at 220 KV, 6 mA and 90 sec. of exposure time.

Fig. 2: Slices and 3D reconstruction of neutron tomography analysis of the sample 8401. Arrows aim at some of the core pins identified.

Fig. 3: Tomographic analysis of the Horus falcon. Upper part of the figure shows the distribution of the inner material through some views of the 3D model and tomographic slices of the center body and tail. Lower part of the figure shows three sections of the tomography with the gray level converted in actual neutron attenuation coefficient (axes scales in pixels; pixel size =107μm)

Fig. 4: a1) and a2) Example of Rietveld refinement of TOF-ND data acquired on bank N.1. The peak positions of measured phases are marked by vertical lines: B = bronze (copper based solid solution), L = lead, C = cuprite, A = algodonite. b) Comparison of three TOF-ND patterns measured on three sites of the falcon. Arrows aims at possible hydoxyapatite peaks, whereas the stars marks possible natrite peaks (see text for discussion). The diffractograms have been vertically shifted for clarity.

Fig. 5: Examples of LIPS elemental depth profiles.

Fig. 6: Comparison of the NRCA spectra measured on the heads of the two bronze figurines. The insert shows portion of the spectra with neutron resonances energies on the abscissa.

Fig. 7: Tomographic analysis of the Neith figurine. On the right the 3D visualization of the reconstructed volumes. Arrows aim at identified core pins.

Fig. 8: Tomographic analysis of the Isis Lactans figurine. Arrows aim at two of the three core pins identified.

Fig. 9: a) XRD analysis on a black/reddish area in the back of the Isis figurine. Symbols mark the diffraction peaks of tenorite (CuO) and cuprite (Cu_2O). b) Raman spectroscopy measurement on the core pin sited in the chest of the Isis statuette (see Fig. 8).

Fig. 10: Details of the gilding traces as seen with optical microscope (right) and ESEM (lower left)

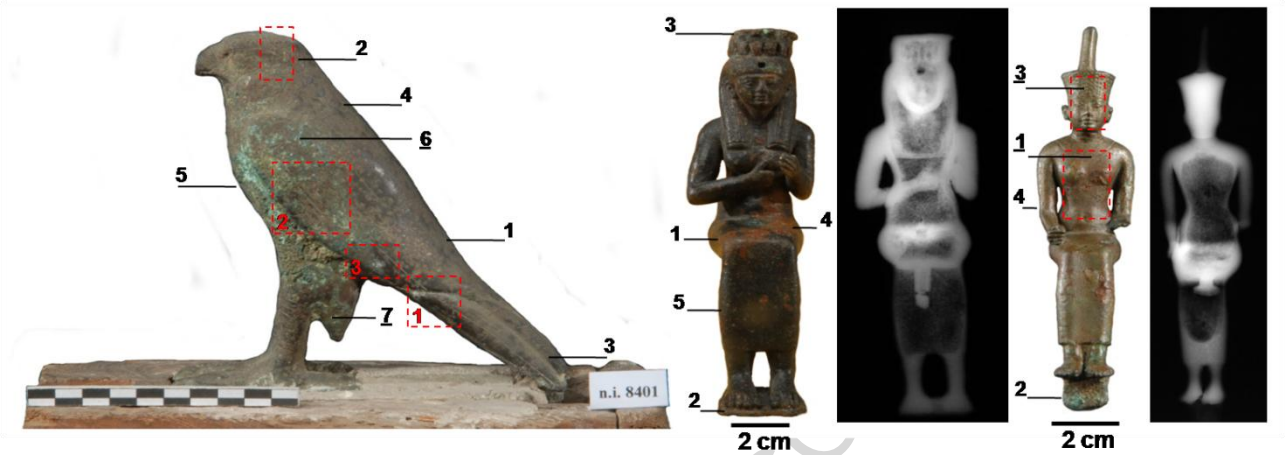

Figure 1

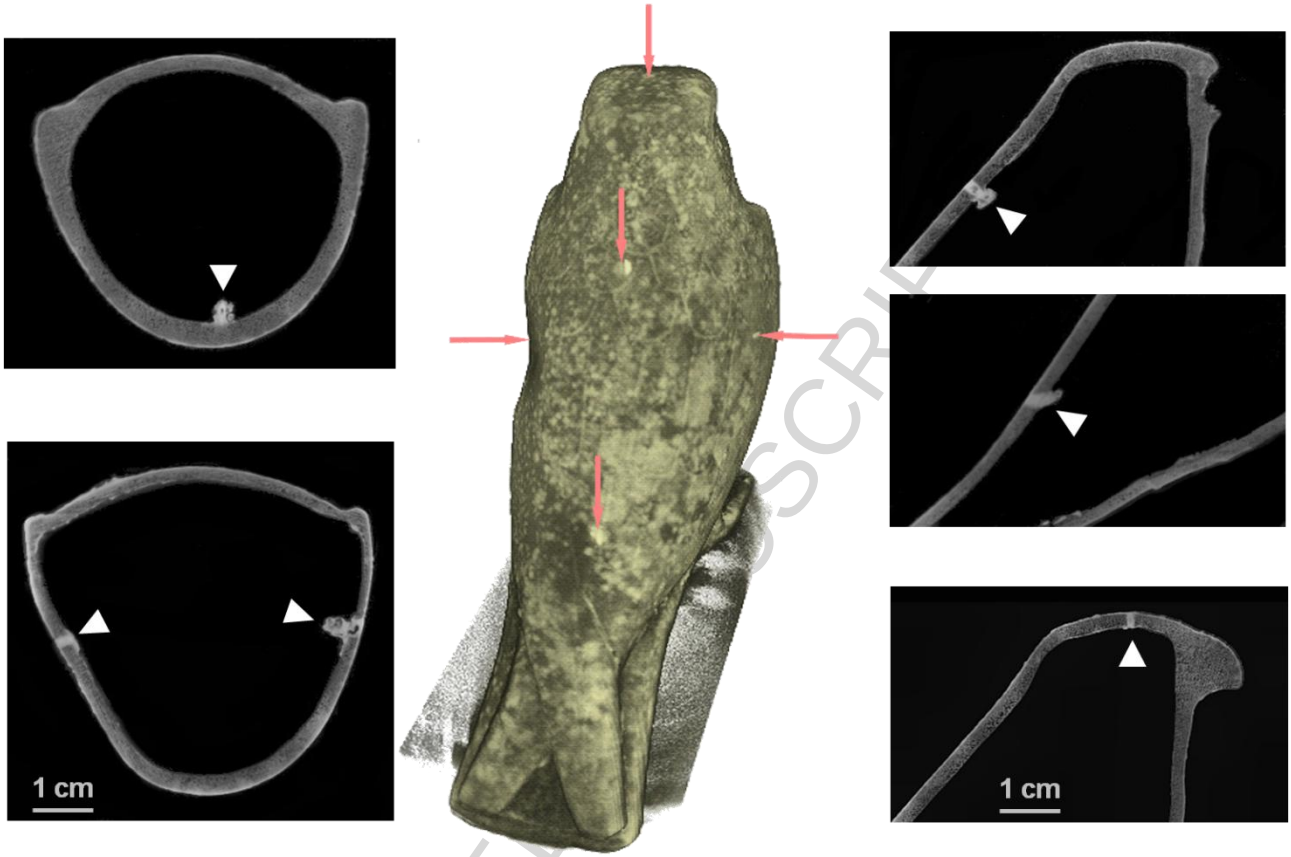

Figure 2

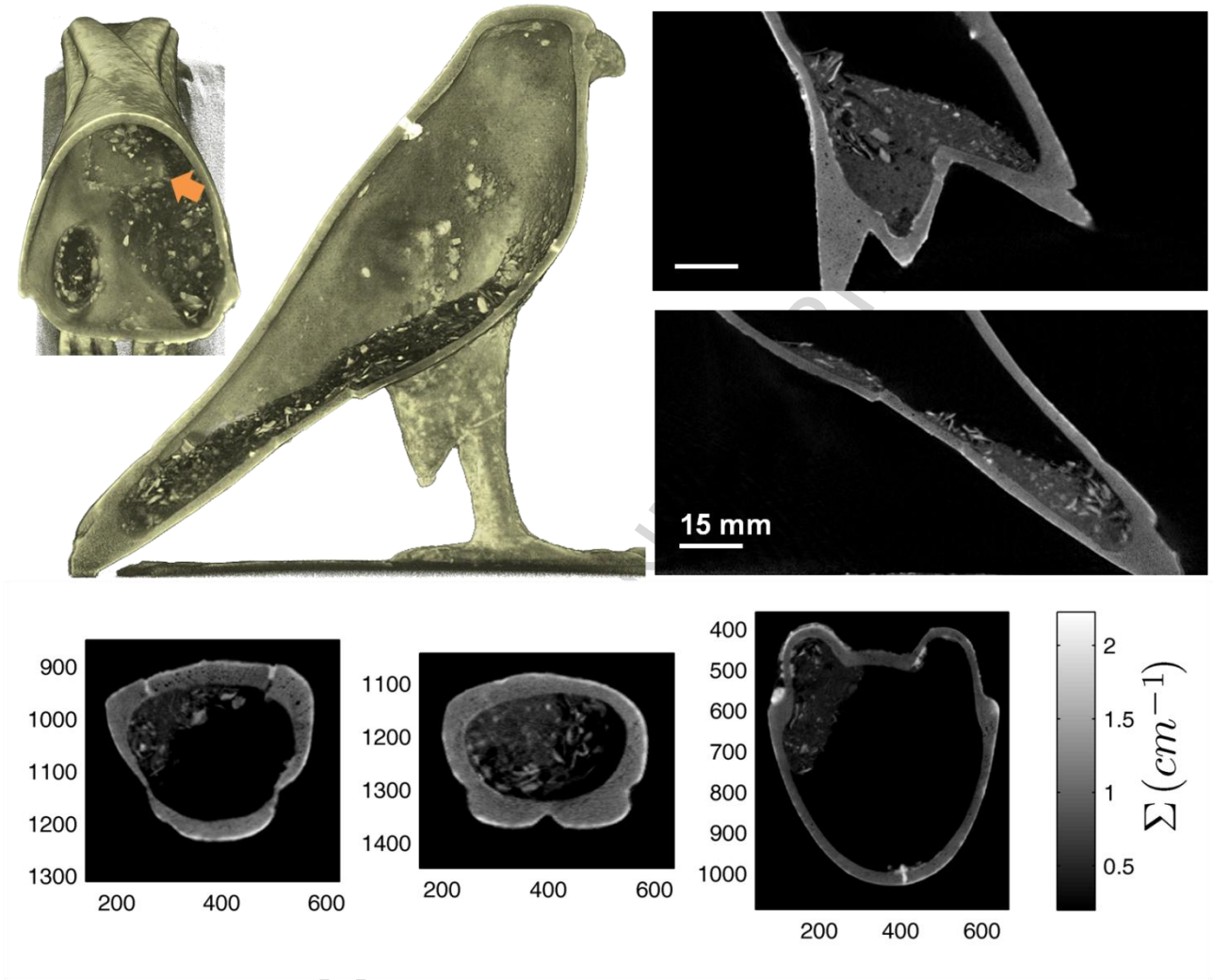

Figure 3

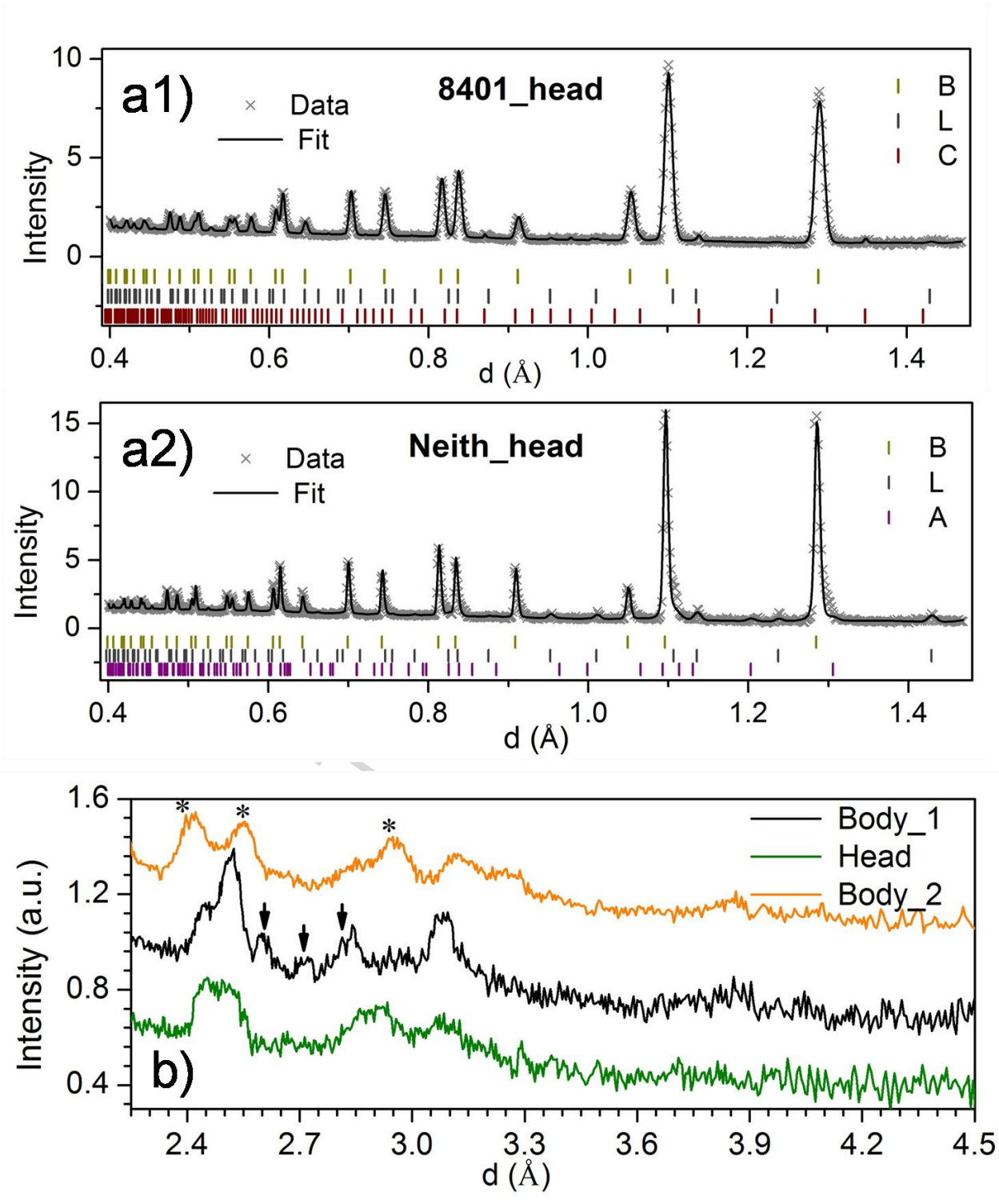

Figure 4

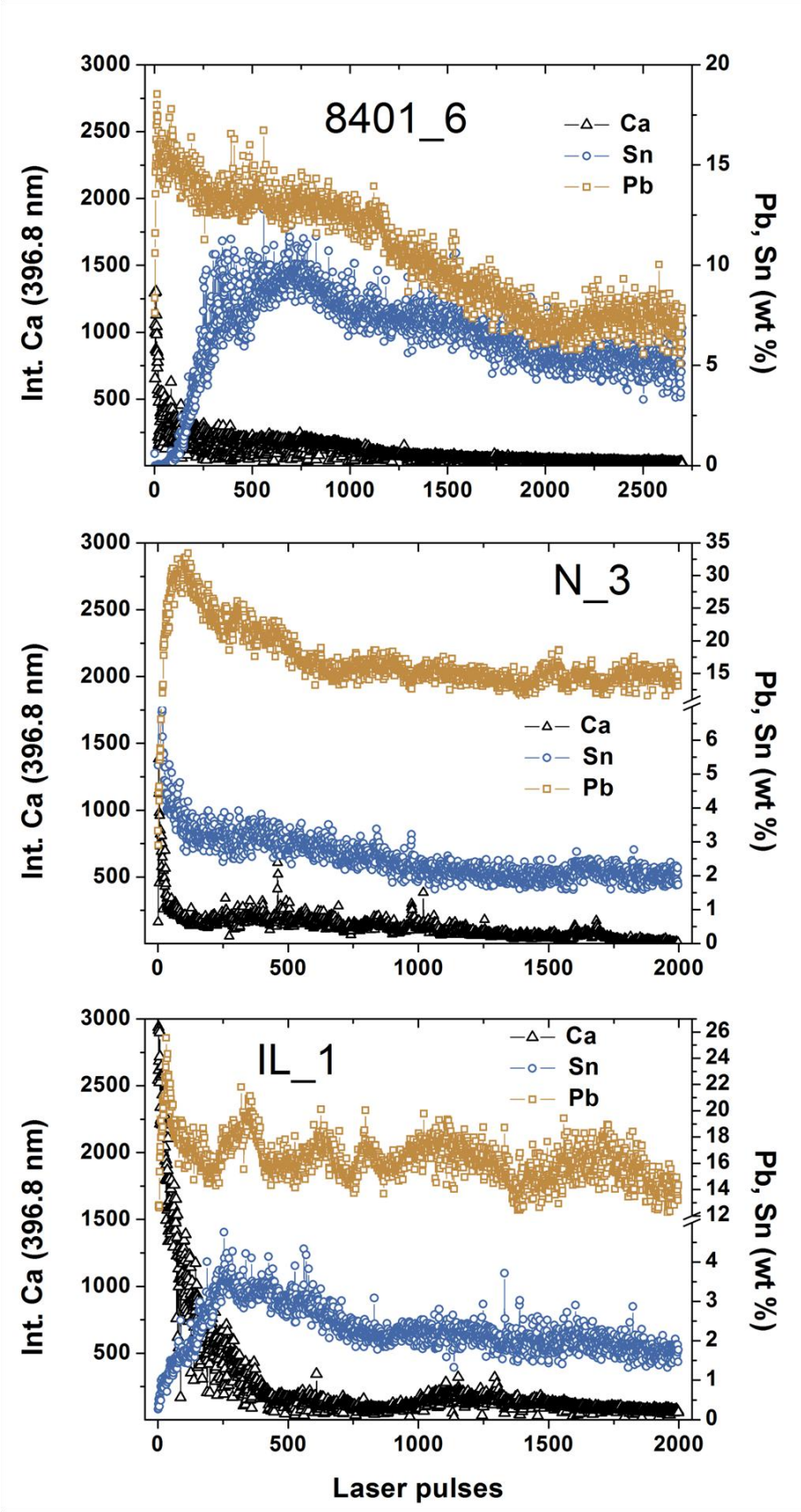

Figure 5

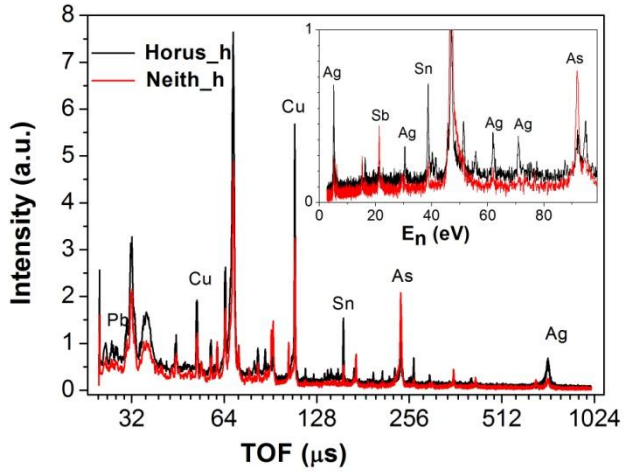

Figure 6

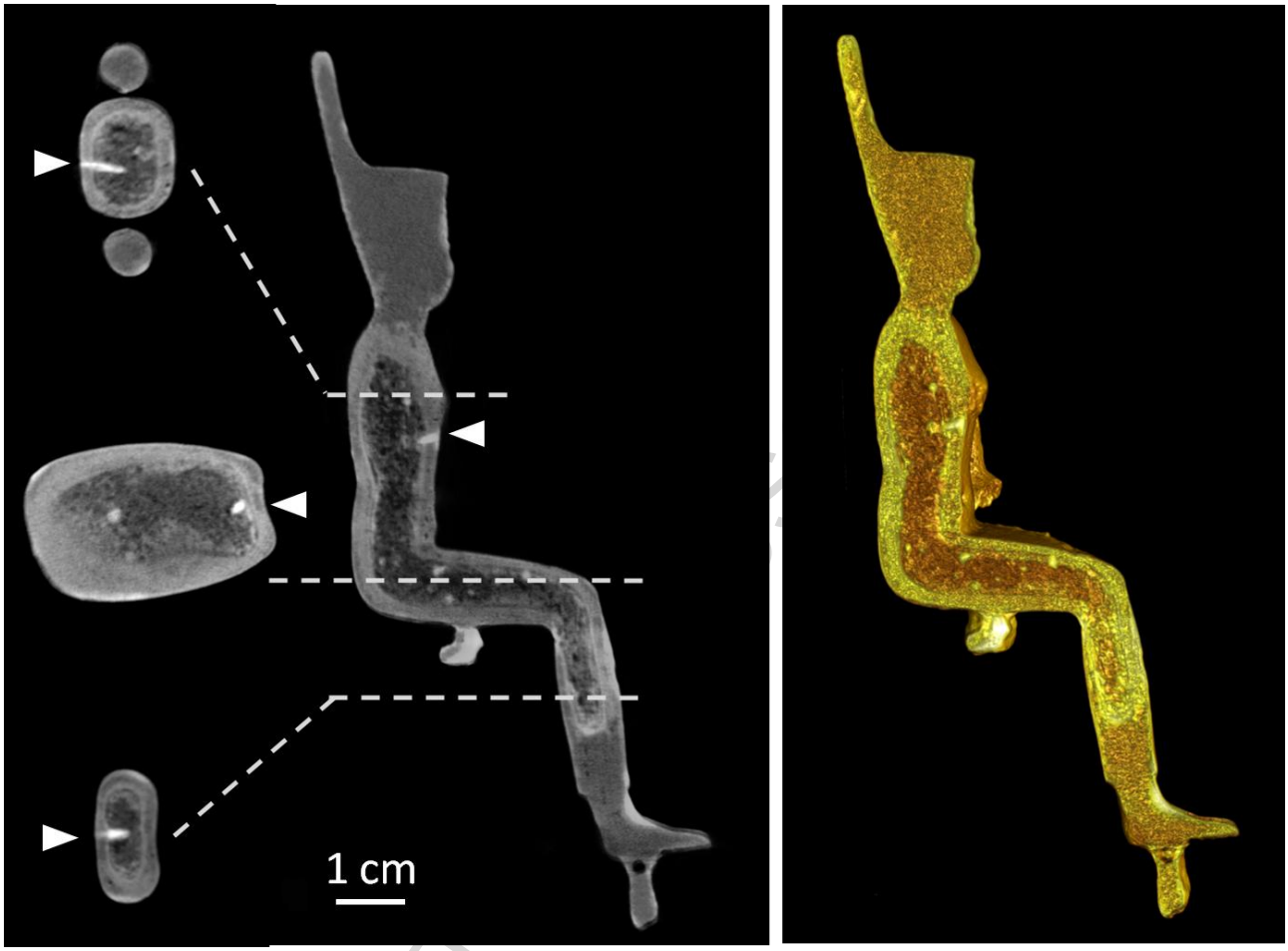

Figure 7

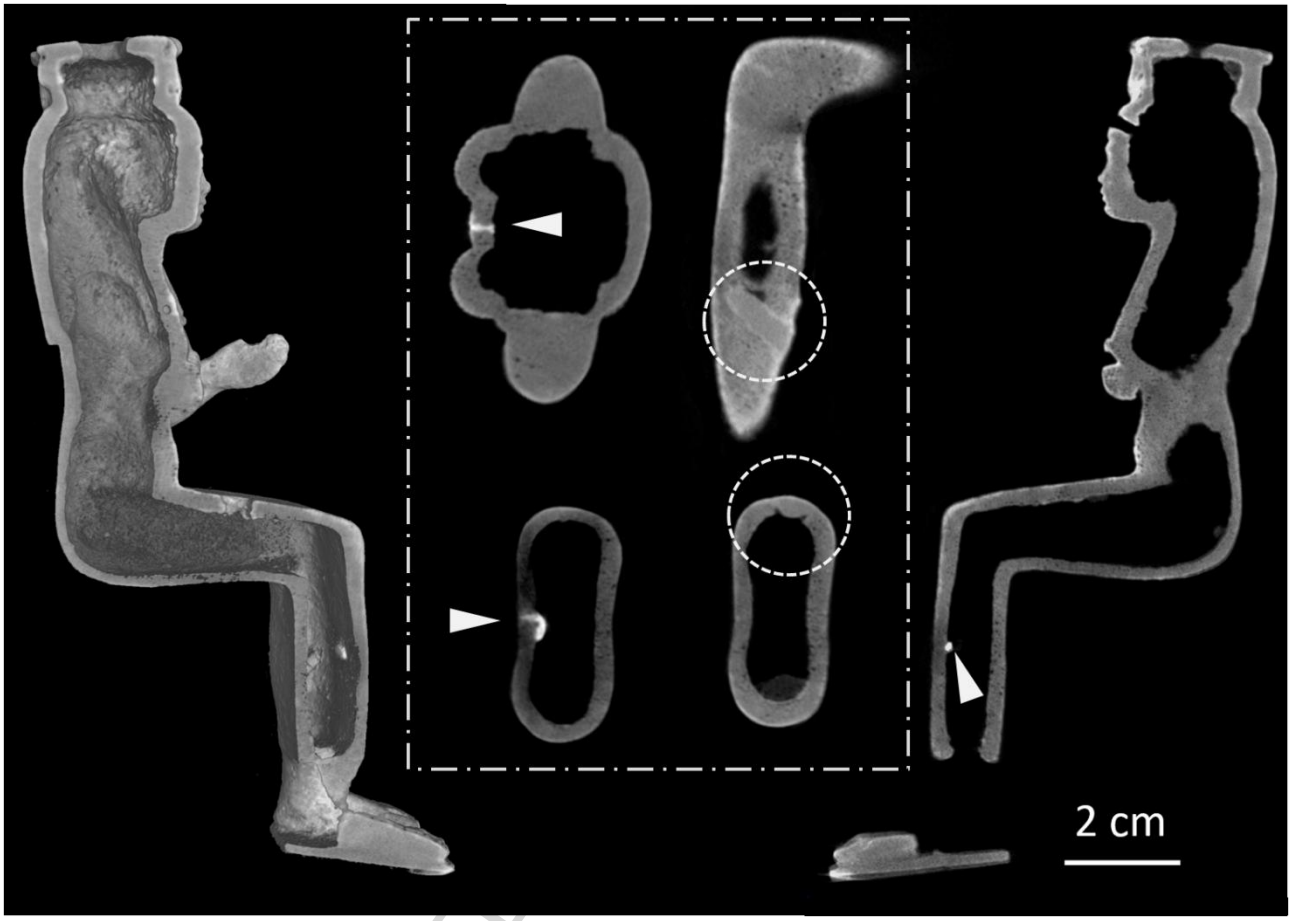

Figure 8

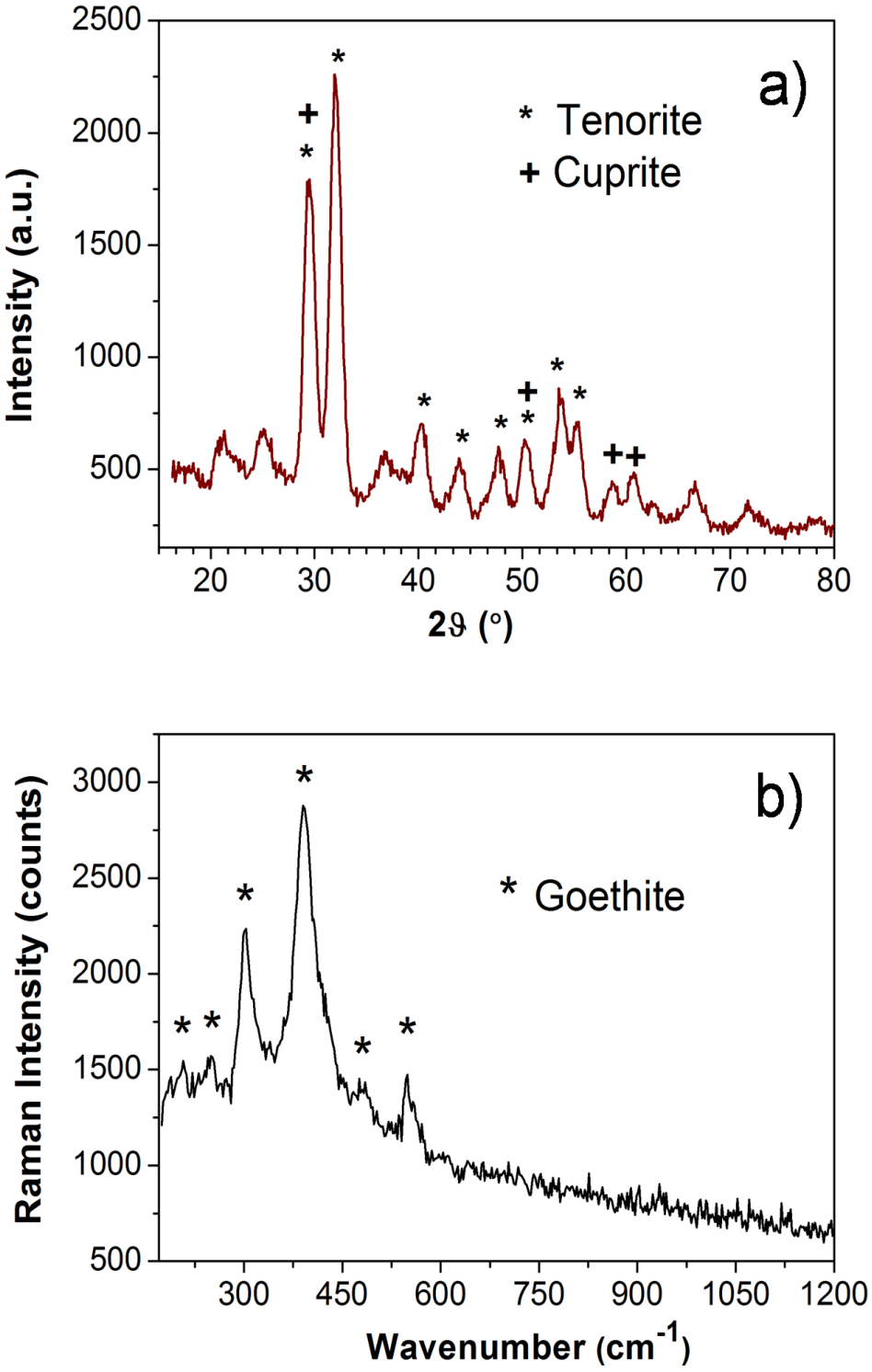

Figure 9

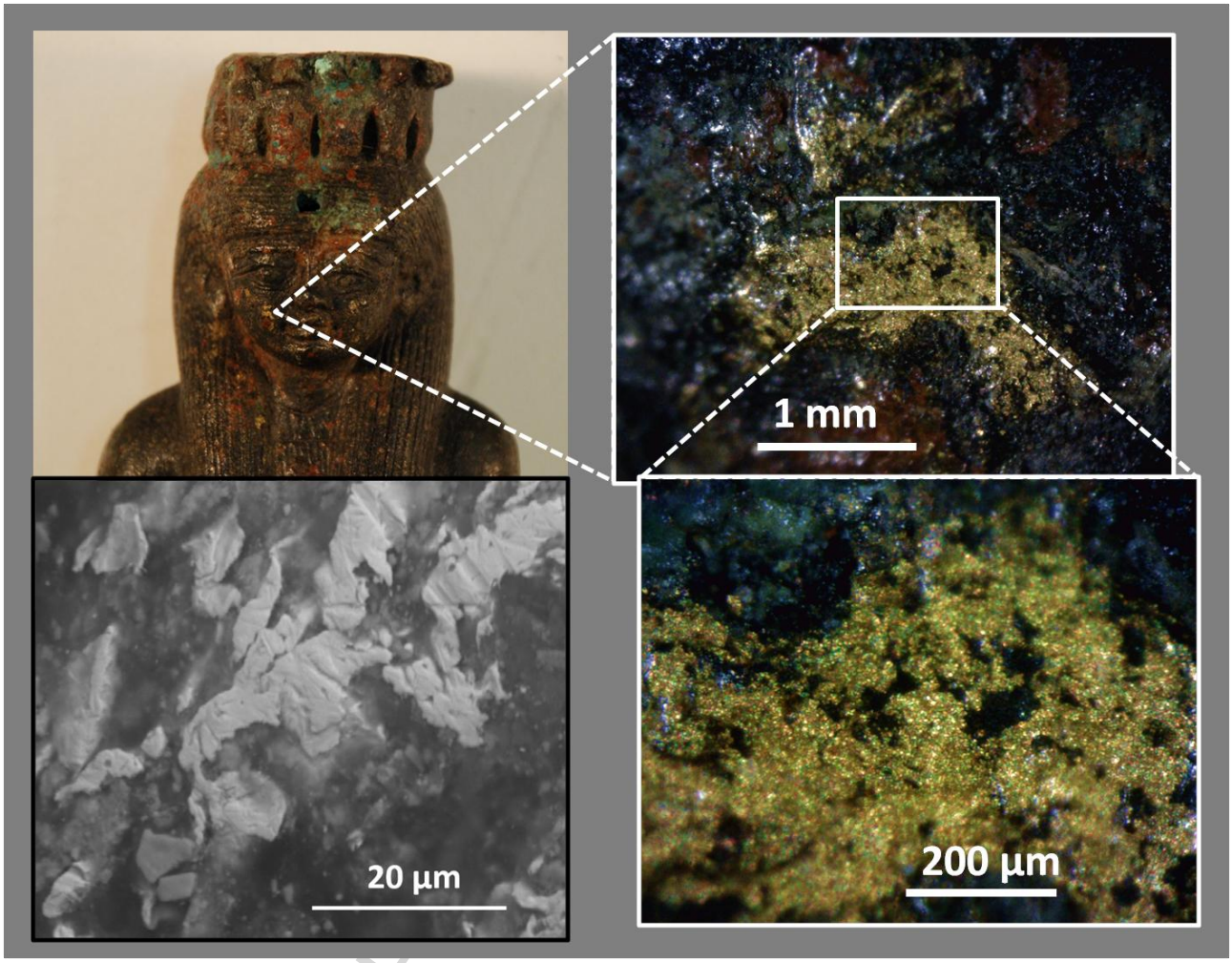

Figure 10

Highlights

Multi-analytical characterization of archaeological Egyptian bronze figurines

Combination of neutron tomography with neutron, laser and X-ray non-invasive compositional analysis

Quantification of complex copper alloy composition and characterization of corrosion products in archaeological bronzes

Archaeometallurgical studies involving hollow-cast archaeological bronzes